Eur. Phys. J. C 10, 249–263 (1999)
Digital Object Identifier (DOI) 10.1007/s100529900113

THE EUROPEAN PHYSICAL JOURNAL C

Comprehensive evidence for a narrow $p\overline{p}$ state of mass 2.02 GeV/c^2

A. Ferrer[1], A.A. Grigoryan[2], V.F. Perepelitsa[3,4], P. Sonderegger[4]

[1] Departamento de Física Atómica Molecular y Nuclear, University of Valencia and IFIC, Centro Mixto University of Valencia – CSIC, Avda. Dr. Moliner 50, E-46100 Burjassot, Valencia, Spain
[2] Theoretical Department, YerPhI, Yerevan Physics Institute, Br. Alikhanian st. 2, 375036 Yerevan, Armenia
[3] ITEP, B. Cheremushkinskaya 25, 117259 Moscow, Russia
[4] CERN, CH-1211 Geneva 23, Switzerland

Received: 26 May 1998 / Revised version: 26 March 1999 / Published version: 3 August 1999

Abstract. We review earlier results, and add new evidence, on the existence of a narrow $p\overline{p}$ state at a mass of 2.02 GeV/c^2, which is seen in six different final states, produced via baryon exchange in π^+p (π^-p) interactions at 20 (12) GeV/c. The data come from a new analysis of the WA56 experiment done at the CERN Omega spectrometer. The 2020 peak is produced near mid-rapidity, in a kinematic region not explored before in baryon exchange processes. Agreement is found with an earlier observation of this state, and its absence in a series of unsuccessful searches is explained. Very low upper limits on mesonic decays of this state favor its interpretation as a baryonium candidate.

1 Introduction

In 1977, Benkheiri et al. published evidence for two narrow $p\overline{p}$ states of masses 2.02 and 2.20 GeV/c^2 [1] produced in a baryon exchange experiment done in the Omega spectrometer at CERN (see Fig. 1a), at 9 and 12 GeV/c beam momentum, via the reaction

$$\pi^- p \to p_f \pi^- [p\overline{p}]. \quad (1)$$

Here and in the following, p_f is a fast forward proton identified by Cherenkov counters, and the $p\overline{p}$ system showing one or more peaks is enclosed in square brackets. The signals appeared to originate preferentially from the quasi-two-body baryon exchange processes shown in Fig. 2a, with a $\Delta(1232)$ or N(1520) baryon going forward.

These utterly unexpected states were statistically significant (7.6 (6.5) standard deviations for the 2020 (2200) peak according to [1]; but see Sect. 3 and (11) for differing definitions of the significance). They were tentatively identified to be baryonia, exotic states strongly coupled to $N\overline{N}$ channels. A number of baryonium searches involving baryon exchange followed [2–6]. Among these, the WA56 experiment [2] had the main purpose of verifying the peaks of [1], assuming the production mechanism of Fig. 2a. It used again the Omega spectrometer, which meanwhile had been upgraded with proportional and drift chambers, and equipped with more particle identifiers (see Fig. 1b and Sect. 2.1). Layout and trigger were optimized for baryon exchange, and were used to collect a large event sample of the reaction

$$\pi^+ p \to p_f \pi^+ [p\overline{p}] \quad (2)$$

at 20 GeV/c, which was expected to yield the richest harvest. Also, reaction (1) was studied at 12 GeV/c in order to reproduce the results of [1]. Neither this nor any of the other experiments did confirm either of these states, nor did they find other baryonium states. Consequently, the subject dropped out of sight, and the peaks of [1] were forgotten.

More recently, we have undertaken a broader analysis of the data of WA56, which to this day remains the richest collection of accurately measured baryon exchange events in its momentum range. We had noted the importance of central production of meson resonances [7], with one pion going backwards in the c.m., and the forward going proton signalling baryon exchange, according to the diagram of Fig. 2b, in the reaction

$$\pi^+ p \to p_f \pi^+ \pi^- (\pi^+_s). \quad (3)$$

We focused therefore on new topologies, with one slow pion accompanying a $[p\overline{p}]$ system, produced centrally via the double baryon exchange process (see Fig. 2c for the double Δ exchange). While more powerful in most respects, the WA56 apparatus was not well equipped for backwards and sidewards emitted particles (which play a minor role in the originally assumed mechanism of Fig. 2a). Therefore the new production reactions are most often characterized by one slow pion, neutral or charged, going undetected. Such events are well identified and separated from the background, thanks to a good missing-mass (MM) resolution of $\delta\sigma(\mathrm{MM}^2) \simeq 0.05\,\mathrm{GeV}^2/\mathrm{c}^4$.

We fitted 3- and 4-prong 1-C final states to the most straightforward related topologies which include a missing

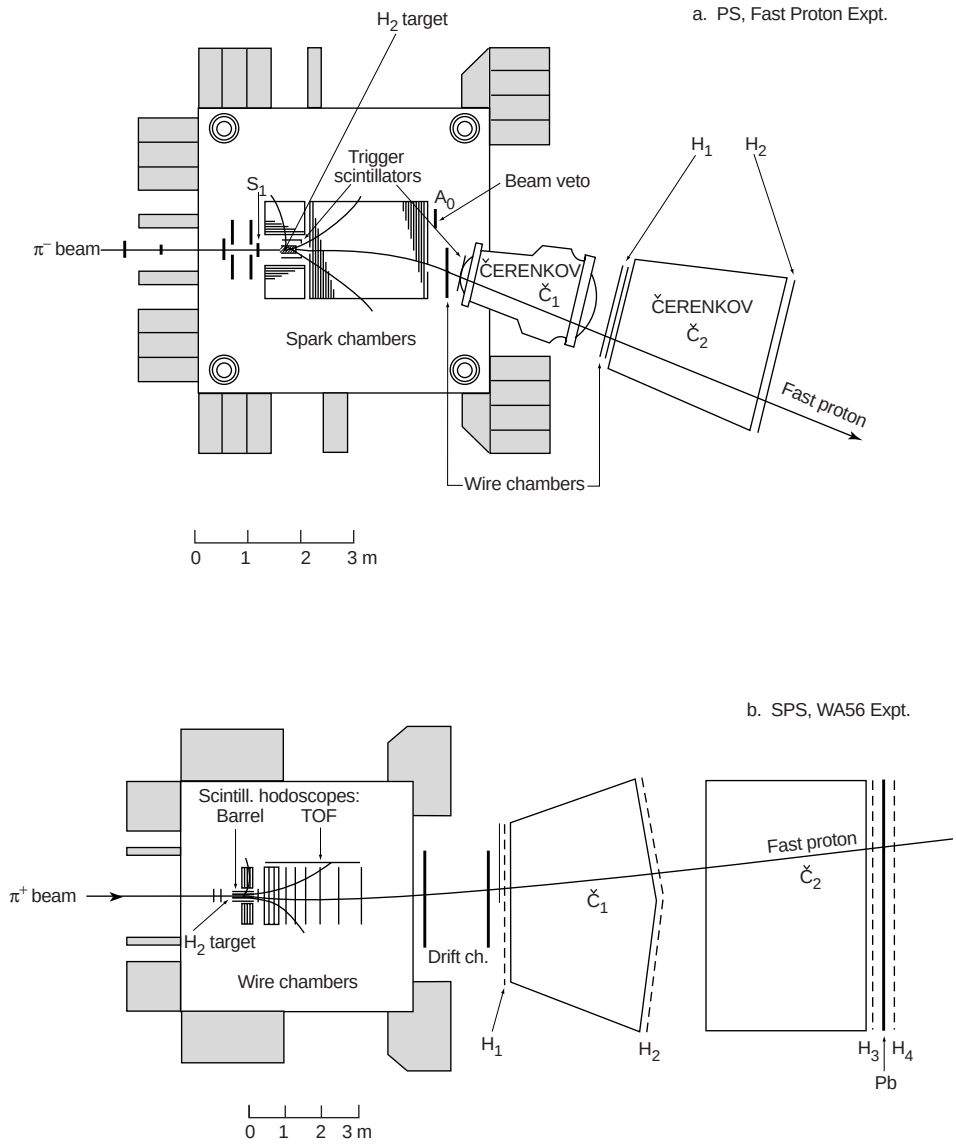

Fig. 1a,b. Layout of the Omega spectrometer, as used **a** in the fast-proton experiment of Benkheiri et al. [1], done at the PS, and **b** in the WA56 experiment at the SPS ([2] and this work). Relevant differences: (i) the first of the two Cherenkov counters was a high-pressure counter in [1], ensuring a rather pure fast-proton trigger at 9 and 12 GeV/c; in [2], the two atmospheric-pressure counters produced a very pure fast-proton trigger at 20 GeV/c, while there was a strong admixture of fast K^+ at 12 GeV/c; (ii) the tracking around the target, quite complete with spark chambers in [1], but insufficient in [2], due to incomplete coverage with wire chambers; (iii) a rich equipment for particle identification in [2], while in [1] only the fast proton was identified

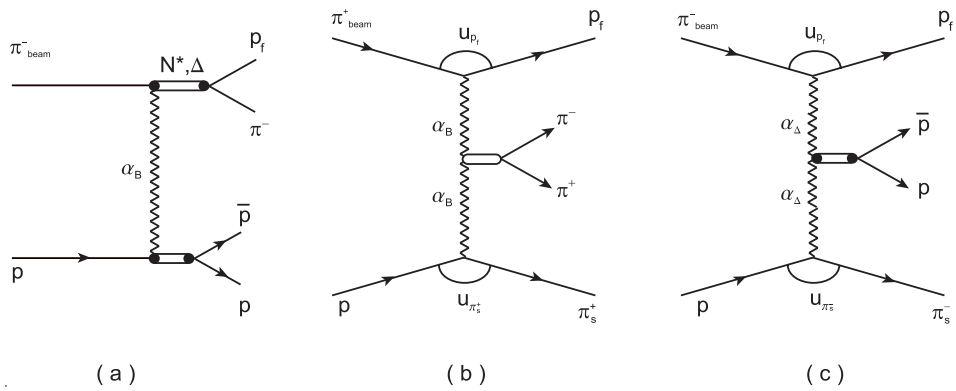

Fig. 2a–c. Diagrams for examples of relevant processes: **a** backward production of a $p\bar{p}$ state in π^-p interactions; **b** central production of an (ordinary) meson in π^+p interactions; **c** central production of a $p\bar{p}$ state in π^-p interactions via double Δ exchange

charged or neutral slow pion:

$$\pi^+ p \to p_f[p\bar{p}](\pi_s^+), \quad (4)$$

$$\pi^+ p \to p_f \pi^+[p\bar{p}](\pi_s^0) \quad (5)$$

at 20 GeV/c and

$$\pi^- p \to p_f[p\bar{p}](\pi_s^-), \quad (6)$$

$$\pi^- p \to p_f \pi^-[p\bar{p}](\pi_s^0) \quad (7)$$

at 12 GeV/c. The round brackets enclose slow pions that are not detected by the Omega apparatus but are reconstructed imposing 1-C kinematic fits. Preliminary results of this investigation have been presented in [8,9]. Furthermore, the 5- and 2-prong reactions:

$$\pi^+ p \to p_f \pi^+ \pi^+[p\bar{p}](\pi_s^-), \quad (8)$$

$$\pi^+ p \to p_f \pi_s^+[(MM \to \text{neutrals})] \quad (9)$$

are presented for the first time, the last one in Sect. 5, reaction (8) together with the reactions (4)–(7) in 2.2–2.5.

The results may be summarized as follows:

- in each of the six topologies, the 2020 peak is found with the correct mass and width, and significances ranging from 3.5 to 7 standard deviations (often thanks to favorable cuts; see Sect. 3);
- when imposing the extra constraints provided by the particle identifiers, the event numbers decrease by varying amounts, but the signal-to-background ratios are maintained or improved, reinforcing the credibility of the results (also Sect. 3);
- the 2020 peak is near-centrally produced, $-1 \leq y_{cm}^{p\bar{p}} \leq 0$ (Sect. 4);
- upper limits on several mesonic decay modes of the 2020 state are obtained, which are low enough to support the hypothesis that it is a baryonium candidate (Sect. 5); indeed, exotic mesons strongly coupled to baryons and decoupled from mesons appear in a large variety of theoretical models (see [10–16]);
- when old and new results are analyzed in the light of the central production mechanism, a consistent quantitative picture of the cross sections of the 2020 peak published by the Omega experiments emerges (Sect. 6);
- indications of a peak at 2.02 GeV/c^2 are found in a number of other production experiments, and are compatible with our cross sections and/or other properties (Sect. 6);
- our results are compatible with the non-observation of the 2020 state in formation experiments provided it is very narrow ($\Gamma \leq 1$ MeV/c^2);
- the 2200 MeV/c^2 state of Benkheiri et al. [1] has not been seen again, neither by us nor in other experiments.

We conclude (Sect. 7) that at the time when both the Omega spectrometer and the LEAR facilities have been closed down, the 2020 peak has enough credibility as a baryonium candidate to serve as a challenge to future hadron physics facilities.

2 Experimental aspects

We describe here the aspects of the Omega apparatus relevant for this work, and more specifically its differences with respect to the setup used for the original claim of two baryonia, and the devices used for particle identification. We then describe the event selection, and in particular the cuts which allowed us to see the 2020 peak with some confidence. These cuts are somewhat simpler than those used in earlier versions of this study [8,9]. Still, while some cuts are quite natural, others are of an ad hoc nature, waiting for a justification by physics.

2.1 Setup and exposures

Figure 1a shows the layout of the Omega spectrometer as used in the earlier experiment [1], and Fig. 1b the one of WA56 [2]. Both used a fast forward proton trigger, defined by a directional (matrix) coincidence from two hodoscopes which encompassed two multicell Cherenkov counters, with no signal in the latter. Counters C2 of Fig. 1a and C1 of Fig. 1b had thresholds for pions, kaons and protons at $p_\pi = 2.8$, $p_K = 9.8$ and $p_p = 18.8$ GeV/c. The thresholds of C2/WA56 were a factor 2 higher, while those of the high-pressure Cherenkov (HPC) C1 of [1] had been about a factor 2 lower.

The data discussed here come from $\pi^- p$ runs at p_{beam} = 12 GeV/c and $\pi^+ p$ runs at 20 GeV/c. We use only events with fast-proton momentum p_{p_f} greater than 6 and 10 GeV/c, respectively. The 20 GeV/c π^+ data show a very good rejection efficiency against forward π^+ and K^+. Indeed, for 4-p 4-C fits to $\pi^+ p \to X_f^+ X^- \pi^+ p$, the squared "Ehrlich mass" m_X [17] has a peak at m_p^2, of resolution $\sigma_{m^2} = 0.028$ (GeV/c^2)^2, which contains 88% of the events, along with 6% at m_K and 6% at m_π (the latter two correspond to much higher cross sections, confirming the excellent efficiency of the Cherenkov counter). The 12 GeV/c data of WA56 had, however, a strong admixture of forward K^+ triggers, to be discussed in Sect. 2.2. The HPC had killed these in the earlier experiment, but was not used in the WA56 experiment, designed originally to run at 20 GeV/c only.

The WA56 experiment made use of a rich detector equipment to tailor the trigger to the topologies of Fig. 2a, including multiplicity requirements in the "barrel" and Cherenkov hodoscopes (see [2] for details). Events containing negative tracks of momentum above 2.8 GeV/c were vetoed unless they were identified as π^-, to help to suppress a diffractive background with fast antiprotons from processes like $\pi^\pm p \to p_f \bar{p} \pi^\pm p_s$. All trigger conditions were incorporated in the simulations used to compute the experimental acceptances.

The WA56 nominal sensitivities used here are based on part of the original WA56 data, and are 150 (30) events/nb for the $\pi^+ p$ ($\pi^- p$) exposure; the acceptances required to derive cross sections from event numbers are dealt with in Sect. 4.

Other particle identifiers were used in WA56, in addition to the Cherenkov counters. The time-of-flight system

TOF was made of 17 scintillator slabs and covered an area 250 cm long and 106 cm high, at 135 cm from the beam axis alongside the forward chambers. It intercepted part of the forward emitted particles of the same charge as the beam, and of momenta roughly between 0.4 and 2.5 GeV/c. With its measured time resolution $\sigma = 0.7$ ns, it allowed p/π^+ ($\overline{p}/\pi^-$) separation from 0.4 to 2.0 GeV/c in π^+p (π^-p) reactions. In the π^-p exposure, the TOF provided $\overline{p}/K^-$ separation up to 1.5 GeV/c momentum.

A 24-element cylindrical scintillator hodoscope ("barrel") of 4 cm radius, 4 mm thickness and 62 cm length surrounded the 60 cm long hydrogen target, protruding 1 cm on each end. For most of the time, the scintillator slabs were equipped with pulse height analyzers, which achieved an average dE/dx resolution of 30%, allowing separation of p and $\overline{p}$ from π up to 1.0 GeV/c, and K from π up to 0.5 GeV/c, with reasonable efficiency. The barrel information was further used to detect the slow charged pions $\pi_s^{\pm}$ from reactions (4) and (6), whose tracks were not reconstructed in the chambers, and eventually identify them.

The use of the response of these particle identifiers has been crucial for confirming the validity and quality of the assignments of the events to given reactions (see Sect. 3).

The mass resolution for the centrally produced $p\overline{p}$ system in 1-C fit events is of order $\sigma_{M[p\overline{p}]} = 10$ to 18 MeV/c^2, as found in a similar study of the centrally produced ϕ meson (a convenient calibrator with its narrow width $\Gamma_\phi = 4.4$ MeV/c^2) [18], and in the experimental fits reported hereafter. Monte Carlo simulation found $\sigma_{M[p\overline{p}]} = 10$ to 12 MeV/c^2, assuming $\Gamma_{2020} = 10$ MeV/c^2. The background was not simulated, except when a model was available, in particular for diffractive production.

2.2 Background in the π^-p data from non-baryon exchange reactions

The π^-p exposure at 12 GeV/c was done without the high-pressure Cherenkov counter which had excluded both pions and kaons above 6 GeV/c from the trigger of Benkheiri et al. [1]. The dominating background comes therefore from the events triggered by a fast forward K_f^+. In the 4-prong 4-C sample, the Ehrlich mass analysis analogous to the π^+p exposure yields as many fast kaons as fast protons (46% each), together with 8% pions. Doubly charged strangeness exchange ($\pi^- \to K_f^+$) is a very rare process. Singly charged strangeness exchange dominates, with a strong $K(892)^0 \to K_f^+\pi^-$ signal present in the various channels, as seen in Fig. 3b for the 4-prong sample.

In this exposure, the TOF system intercepts negative particles. It is used to exclude henceforth all π^-p events from reactions (6) and (7) which had an identified K^-. This removes part of the K_f^+ triggers, thereby improving the signal-to-background (S/B) ratio.

2.3 Selection of 1-C and 2-C events with one missing pion

Our results come mainly from data samples corresponding to 3-prong events of $++-$ topology (with one charged track undetected), 4-prong charge-balanced events with missing neutral(s), and 5-prong events of $++++-$ topology, again with one charged track undetected. For these events, the missing mass squared (MM^2) was calculated with appropriate mass hypotheses for the detected particles. The mass assignments were required to be in accordance with Cherenkov counter information available for high-momentum particles. Clear signals of lost π_s^+, π_s^0 and π_s^- were seen, as illustrated by Fig. 3a in the case of reaction (4). The events were selected if they were inside the m_π^2 band, namely $|MM^2 - m_\pi^2| < 0.16$ (0.12) (GeV/c^2)^2 in exposure at 20 (12) GeV/c. Then a 1-C momentum-energy balance fit was performed. For the analysis presented here we retained those events (about 50% of the ones in the m_π^2 band) which passed the 1-C kinematic fit with χ^2 probability $P(\chi^2) > 5\%$.

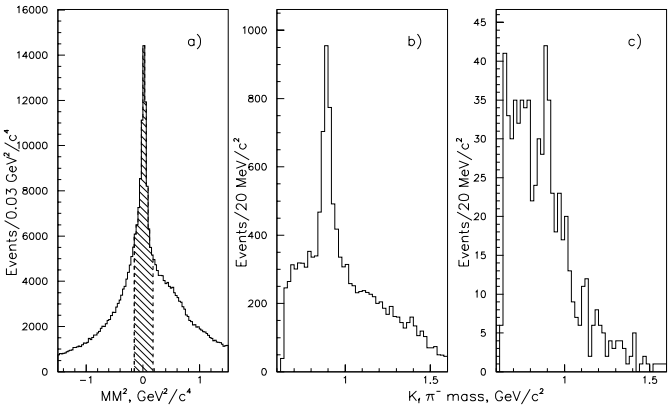

Fig. 3. a Missing-mass spectrum for events of $++-$ topology in the 20 GeV/c π^+p exposure; the dashed band corresponds to the events which were fed into 1-C kinematic fit (see text); **b** $K_f^+\pi^-$ mass in 12 GeV/c π^-p events of 4-prong topology which passed the 1-C fit to $p_f\pi^-p\overline{p}\pi_s^0$; **c** the same, after the $\overline{p}$ being identified by TOF

Also, for reactions (4) and (6) we studied subsamples of events in which a kinematically recovered π_s^+ or π_s^- was detected by the appropriate barrel strip, corresponding to an accuracy in azimuthal angle of $\sigma_\phi = 5°$. This selection suppresses backgrounds originating from reactions with more than one particle lost. The events selected under such conditions (1-C kinematic fit and association of the slow pion with the fired barrel slab) are effectively reconstructed with two constraints, and are called 2-C events for briefness.

2.4 KIN: Kinematic cuts

The following kinematic cuts (denoted KIN in the figure and table captions) were used to suppress the diffractive background and to emphasize the central regions for the $p\overline{p}$ system in reactions (4)–(8):

(i) $\cos\theta_J < 0.6$, where θ_J is the Jackson angle of the $\overline{p}$ in the $p\overline{p}$ rest system, with the z axis taken along the direction of the virtual exchanged baryon, i.e. ($\mathbf{p}_{beam} - \mathbf{p}_{p_f}$) for reaction (4) and (6), and ($\mathbf{p}_{beam} - \mathbf{p}_{p_f} - \mathbf{p}_{\pi^+}$) for reaction (5) and (7). The $\cos\theta_J$ distribution is expected to

be symmetrical in case of $p\bar{p}$ resonance production, while the diffractive background is expected, and was indeed found, to be concentrated in the forward cone.

(ii) A cut $\Delta p = |\mathbf{p}_p| - |\mathbf{p}_{\pi_s}| > \Delta p_{\min}$ was used with $\Delta p_{\min} = 1\,\mathrm{GeV}/c$ for the 3-prong reactions (4) and (6), and $\Delta p_{\min} = 0.8\,\mathrm{GeV}/c$ for the 4-prong reactions (5) and (7). Although meant to isolate the $p\bar{p}$ system from the slow particles, this cut turned out to be rather effective also to suppress background reactions with a slow (spectator) proton[1].

One further and rather ad hoc cut:

(iii) $y_{\pi^+} > y_{p\bar{p}}$ was used for the $\pi^+ p \to$ 4-prong reaction (5) only; this requirement leaves the backwards (negative rapidity) region to the $p\bar{p}$ system and the missing π_0.

2.5 ID: Particle identification cuts

We use also particle identification cuts, based on TOF and/or $\mathrm{d}E/\mathrm{d}x$ indications, to select event samples with one or several final state particles identified. A particle was considered to be identified as $p(\bar{p})$, $K^{\pm}$ or $\pi^{\pm}$ if the most probable hypothesis i had a probability (computed from the measured experimental response) $P_i > 4\%$ and if this probability was at least three times greater than the best competing mass hypothesis. In practice, we use the procedure in two cases: either to identify $p(\bar{p})$ against the $\pi^{\pm}$ hypothesis; or, in the $\pi^- p$ data only, to identify a final state K^- against both $\bar{p}$ and π^- alternatives.

We have tested the TOF identification on the $K(892)^0$ peak of Fig. 3b. Only 2% of the peak subsist when the second negative particle is identified as a $\bar{p}$, as shown in Fig. 3c; 8% of the background under the peak subsist. The limited acceptance of the TOF prevents us from generalizing its use. But it may advantageously replace the kinematic cuts, which entail a similar loss in event numbers as the particle identification cuts.

3 The $p\bar{p}$ mass spectra

Before accepting the 2020 peak as a baryonium candidate, we made various checks on a possible origin from the reflection of a misinterpreted non-exotic narrow resonance, with consistently negative results.

There are two global arguments which disfavor a fake peak or a reflection: (i) the 2020 peak is narrow, its width not exceeding 20–30 MeV/c^2, and (ii) as documented below, the extra background reductions obtained by requiring particle identification by one or the other of the available detectors confirm the mass assignments obtained by the kinematic fit. Indeed, the signal-to-background ratio is either maintained or improved, just as had been observed in a similar treatment of the meson resonance events studied in the same experiment [7]. It is never degraded, which would be expected if the original interpretation of the event were contradicted by a more refined treatment.

The $p\bar{p}$ mass spectra have been parameterized throughout as

$$A(M - M_0)^{\alpha} \exp\{(M_0 - M)\beta\}(1 + \gamma \mathrm{BW}), \qquad (10)$$

where $M_0 = 2m_p$, and BW represents a Breit–Wigner term taken as

$$\mathrm{BW} = \frac{\Gamma^2/4}{(M - M_R)^2 + \Gamma^2/4}$$

We have also tried fifth-order polynomials for an alternative background description used to evaluate the systematic uncertainties; the polynomial fit tended to decrease the background yields.

For statistics, we sum the number N of events observed in the interval $2.00 < M_{p\bar{p}} < 2.03\,\mathrm{GeV}/c^2$, which best encompasses the peak. (For the 1-C samples of the $\pi^+ p$ data, we sum over 4 rather than 3 bins of 10 MeV/c^2.) The signal S is then given by $S = N - B$, where B is the fitted background in the same interval. The statistical significance is given in standard deviation units, the standard deviation for a narrow signal over a wide and smooth background being defined as

$$\sigma_S = \sqrt{N}. \qquad (11)$$

We prefer this more conservative definition to the one used by Benkheiri et al. [1], $\sigma_S = \sqrt{B}$.

3.1 $\pi^+ p$ exposure, $p_{\mathrm{beam}} = 20\,\mathrm{GeV}/c$

The $p\bar{p}$ mass spectra from reactions (4) and (5) are shown in Fig. 4, before and after applying kinematic cuts. Peaks at a mass close to 2.02 GeV/c^2 are clearly seen. The signal to background ratios are small, but the statistical significance of the peaks is high.

The kinematic cuts (i) and (ii) ("KIN") preserve most of the signal for the 3-prong reaction (4), while eliminating more than 50% of the background, as can be seen by comparing Fig. 4a (all 1-C events) and 4b (after KIN cuts). A further improvement is obtained by constraining the azimuth of the slow $\pi^{\pm}$ seen in the barrel, while its track is not reconstructed. This is seen by comparing Figs. 4a and 4b (1-C) with Figs. 5a and 5b (2-C). Similar improvements of S/B accompanied by an overall loss of events can be obtained by identifying one or more final state particles. Figure 5c shows the events of Fig. 5a which have both the p and $\bar{p}$ identified. In Fig. 5d all four final state particles were identified, including the π_s^+ (by the $\mathrm{d}E/\mathrm{d}x$ measurement in the barrel). It can be seen that the use of particle identifiers produces an essential improvement of the signal-to-background ratio, as these selections happen to favor the kinematic region of $p\bar{p}$ production where the diffractive background is small. Moreover, as mentioned before, the improvement of the S/B ratio with positive identification of some or all produced particles disproves the hypothesis that the observed peaks could be due to a

[1] We also tried an alternative cut meant to reduce the background not due to central production, requiring $y(p\bar{p}) - y(\pi_s) > \Delta y$, instead of cut (ii), with $\Delta y = 0$, 0.5, 1. Results were comparable, showing a slightly lower S/B ratio

Table 1. Parameters of the resonance fits in the most relevant $p\overline{p}$ mass spectra, indicated by their figure numbers: number of prongs, constraints (C), kinematic cuts (KIN), and particle identifications (ID) (not including the p_f, which is always identified); χ^2/number of degrees of freedom; mass and width of the 2020 peak, each with statistical (fit) errors; events in signal/in background; statistical significance of the peak, expressed as number of standard deviations

Spectrum (Figure)	No. of prongs	Constraints	$\chi^2_{\rm fit}$/ndf	Mass of $p\overline{p}$ state (MeV/c^2)	Width of $p\overline{p}$ state (MeV/c^2)	S/B	n.s.d.
			20 GeV/c π^+p data				
4a	3	1-C	39/55	2009 ± 6	30 ± 12	258/1561	6.0
4b	3	1-C, 2-KIN	38/55	2012 ± 6	34 ± 21	195/687	6.6
4c	4	1-C 1-KIN	51/55	2021 ± 6	35 ± 24	462/3889	7.0
4d	4	1-C, 3-KIN	45/55	2016 ± 7	39 ± 20	201/1214	5.3
5a	3	2-C	57/55	2010 ± 4	17 ± 9	115/599	4.3
5b	3	2-C, 2-KIN	56/55	2009 ± 4	12 ± 10	84/257	4.5
5c	3	2-C, 2-ID	53/55	2014 ± 4	12 ± 8	26/29	3.5
5d	3	2-C, 3-ID	40/55	2013 ± 4	12 ± 10	23/16	3.7
5e	4	1-C, 2-ID	42/55	2018 ± 6	21 ± 18	28/36	3.4
5f	5	1-C	60/55	2010 ± 8	11 ± 7	58/219	3.5
10a	2	2-KIN	61/49	2007 ± 9	42 ± 32	80/388	4.0
10b	2	2-KIN,1-ID	55/49	2020 ± 4	29 ± 24	43/166	3.3
			12 GeV/c π^-p data				
6a	3	1-C, 2-KIN	43/55	2024 ± 5	22 ± 15	60/191	3.8
6b	3	1-C, 1-ID	49/55	2017 ± 4	14 ± 10	29/76	2.8
6c	4	1-C, 2-KIN	73/55	2019 ± 8	10 ± 10	62/363	3.0
6d	4	1-C, 1-ID	69/55	2014 ± 4	13 ± 5	82/165	5.2
			Sum of 2-ID events				
7	3 + 4	1-C + 2-C, 2-ID	92/94	2015 ± 3	10 ± 4	65/89	5.2

kinematic reflection of known resonances of the same pair of particles, e.g. a misidentified ρ meson.

Turning now to the 4-prong reaction (5), the mass spectra of 1-C events are shown on Fig. 4c before and 4d after applying KIN cuts (i) to (iii). The effect of particle identification on the $p\overline{p}$ mass spectrum is shown on Fig. 5e, for 1-C events in which both the p and $\overline{p}$ were identified.

A single $p\overline{p}$ mass spectrum for 1-C events of the 5-prong reaction (8) is shown in Fig. 5f, with no cuts. The 2020 signal is clearly visible. Here again, the KIN cuts double the S/B ratio, but the event numbers become small, and the significance decreases from the 3.5 standard deviations of Fig. 5f to 2.7 σ (figure not shown).

Table 1 shows the resulting BW parameters together with the corresponding χ^2 values and numbers of degrees of freedom, the numbers of signal (S) and background events (B), and the statistical significance of the signal. The obtained widths are compatible with the experimental resolutions. A correlation is seen between the measured peak width and the number of constraints. This effect is not reproduced by the Monte Carlo technique, which simulates only the listed reactions and not the background. It could be explained by observed fact that the background of the 1-C fits contains also 2020 states produced in somewhat different final states, e.g. with more than one missing pion, blurring the peak. Such final states are conserved by the KIN cuts, but rejected by 2-C fits or when identifying final-state particles, which suppresses the yield of events with badly measured track parameters.

3.2 π^-p exposure, $p_{\rm beam}$=12 GeV/c

Figure 6 shows the $p\overline{p}$ mass spectra for events of the reactions (6) and (7) selected with the same kinematic cuts as described above, to maintain the homogeneity of the selection criteria. They are shown at first as 1-C fits with KIN cuts (i) and (ii) for both, the 3-prong (Fig. 6a) and for the 4-prong events (Fig. 6c), and then replacing the KIN cuts by positive identification of the $\overline{p}$ (Figs. 6c and d). Table 1 again gives the parameters of the fits to the mass spectra.

The 4-prong reaction is visibly plagued by the kinematic reflection of the $K(892)^0 \rightarrow K_f^+\pi^-$, as shown in Fig. 3b. We have been able to identify the reaction

$$\pi^-\mathrm{p} \rightarrow \mathrm{K}_f(890)^0 \Lambda(1520)(\pi_s^0) \qquad (12)$$
$$\searrow \quad \searrow$$
$$\mathrm{K}_f^+\pi^- \quad \mathrm{pK}^-$$

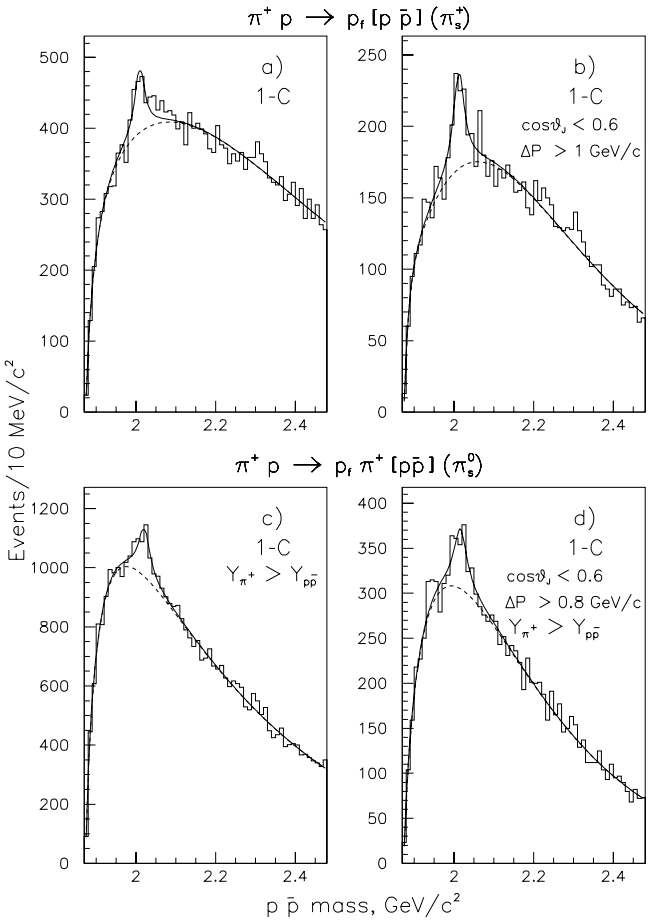

Fig. 4a–d. pp̄ mass spectra for 1-C events from **a** reaction (4), all events; **b** reaction (4), events satisfying the kinematic cuts; **c**, **d** the same as **a**, **b** for events from reaction (5), with the additional kinematic cut $y(\pi^+) > y(\mathrm{p\overline{p}})$. The 2020 peak is wide here, before further constraints are applied; its event numbers are therefore summed over 4 bins of 10 MeV/c^2

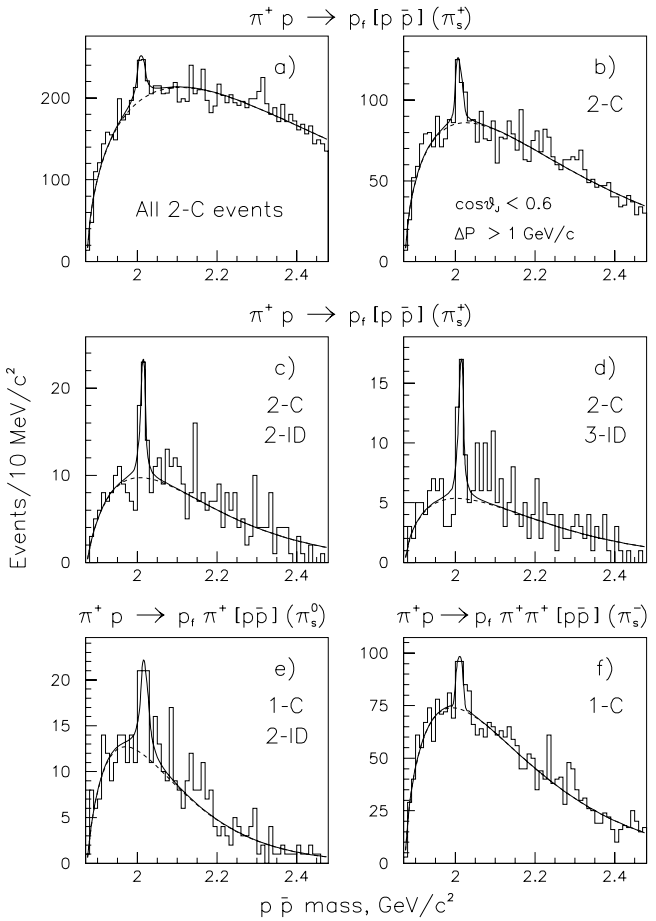

Fig. 5a–f. pp̄ mass spectra for **a** 2-C events from reaction (4); **b** the same for events satisfying the kinematic cuts; **c** 2-C events from reaction (4) in which both p and $\overline{\mathrm{p}}$ were identified (by the barrel and/or TOF hodoscopes; here and in the following figures, "2-ID" means that 2 particles have been identified, in addition to the fast proton); **d** the same events with the π_s^+ being further identified with the barrel $\mathrm{d}E/\mathrm{d}x$ measurement. **e** 1-C events from reaction (5) in which both p and $\overline{\mathrm{p}}$ were identified; **f** 1-C events from reaction (8), no cuts

using and manipulating $\mathrm{K_f^+}\pi^-$ versus $\mathrm{pK^-}$ invariant mass scatter plots, and to show that the misidentified $\Lambda(1520)$ is at the origin of the sharp peak seen near 1940 MeV/c^2 in Fig. 6c. When positive identification of the $\overline{\mathrm{p}}$ is required, the $\mathrm{K}(892)^0$ is largely suppressed, as noted in Sect. 2.5 and seen in Fig. 3b, 3c, and most of the spurious "1940" peak vanishes, as seen in Fig. 6d.

3.3 Combined spectrum with optimal mass resolution

We combine the pp̄ mass distributions of 2-C, 3-prong events of reactions (4) and (6), and 1-C, 4-prong events from reactions (5) and (7), in which both p and $\overline{\mathrm{p}}$ were identified, to obtain a mass spectrum with good statistics and a good signal-to-background ratio ($S/B \simeq 0.7$). It is plotted in Fig. 7 in 5 MeV/c^2 wide bins. The standard Breit–Wigner plus background fit determined the mass and width of the 2020 peak to be $M_{2020} = (2015 \pm 3)$ MeV/c^2, and $\Gamma_{2020} = (10 \pm 4)$ MeV/c^2. These are our most accurate estimates for mass and width of this state. The errors are statistical, and the obtained width is compatible with our experimental resolution. The statistical significance of the peak exceeds 5 s.d.

To conclude this section we remark that the masses and widths given in Table 1 are well compatible with those of Benkheiri et al. [1], (2020 ± 3) and (24 ± 12) MeV/c^2, respectively.

4 Production mechanism and integrated cross sections

We document the rapidity structure of events corresponding to the 2020 peak ($2.00 < M_{\mathrm{p\overline{p}}} < 2.03$) from the 3- and 4-prong reactions (4)–(7) on Fig. 8. The fastest particle ($\mathrm{p_f}$), the pp̄ peak and the undetected pion appear in three distinct rapidity regions. These are well separated for reaction (4) (Fig. 8a); the other reactions show simi-

Table 2. Number of events, acceptances and integrated cross sections times branching ratio for different decay modes of the centrally produced 2020 resonant state

Channel	Decay mode	Number of events or upper limit at 95% CL.	Acceptance (%)	$\sigma_{\rm int}\times$ BR (nb)
20 GeV/c π^+p data				
$\pi^+ p \to p_f p\overline{p}(\pi_s^+)$	$p\overline{p}$	258±43	7.4	23 ± 4
$\to p_f p\overline{p}\pi^+(\pi_s^0)$	$p\overline{p}$	462±66	3.2	95±14
$\to p_f \pi_s^+ +$ neutrals	neutrals	80±20	1.3	41 ±10
$\to p_f p\overline{p}\gamma\pi_s^+$	$p\overline{p}\gamma$	< 2	1.2	< 1
$\to p_f \pi^+\pi^-(\pi_s^+)$	$\pi^+\pi^-$	<20	3.4	< 4
$\to p_f \pi^+\pi^-(\pi^0)\pi_s^+$	$\pi^+\pi^-\pi^0$	<20	1.2	<11
$\to p_f 2\pi^+2\pi^-(\pi_s^+)$	$2\pi^+2\pi^-$	<40	3.8	< 7
$\to p_f K^+K^-(\pi_s^+)$	K^+K^-	<60	4.2	< 10
$\to p_f K^{0*}\overline{K^{0*}}(\pi_s^+)$	$K^{0*}\overline{K^{0*}}$	<80	2.2	<24
12 GeV/c π^-p data				
$\pi^- p \to p_f p\overline{p}(\pi_s^-)$	$p\overline{p}$	60± 16	2.4	84 ± 22
$\to p_f p\overline{p}\pi^-(\pi_s^0)$	$p\overline{p}$	62±21	1.1	195±65
$\to p_f \pi^+\pi^-(\pi_s^-)$	$\pi^+\pi^-$	<5	1.6	<10
$\to p_f \pi^+\pi^-(\pi^0)\pi_s^-$	$\pi^+\pi^-\pi^0$	<4	0.6	<20
$\to p_f 2\pi^+2\pi^-(\pi_s^-)$	$2\pi^+2\pi^-$	<40	2.1	<30
$\to p_f K^+K^-(\pi_s^-)$	K^+K^-	<20	2.2	<20

lar features. The 2020 peak is clearly centrally produced, at slightly negative c.m. rapidities. We note that in double baryon exchange, the projectile quark interacts with a target diquark, and this system is at rest at $y_{\rm cm} \simeq -0.2$, justifying to some extent the slight backward trend of $p\overline{p}$ production.

The distributions of the squared 4-momentum transfer from the beam pion to the fast proton for reactions (4) and (6), u'_{p_f}, and to the fast proton + charged pion system for reactions (5) and (7), $u'_{p_f\pi}$, as well as from the target proton to the slow pion, u'_{π_s} (see Fig. 2), within the same M_{2020} band, are exponential, with negative slopes in the range of 2–3 (GeV/c)$^{-2}$, similar to what was found for central production of the ρ^0, f_2 and ρ_3^0 mesons [7]. The angular distributions of the 2020 peak were found to be consistent with isotropy in the Gottfried–Jackson frame defined in Sect. 2.4, after subtracting an appropriate background derived from neighboring mass bands.

Using these u' dependences and isotropic angular distributions of the $p\overline{p}$ state decays, we have calculated the total acceptances of the experiment for reactions (4)–(7) (see Table 2). The number of events under the observed peaks were obtained by subtracting the background as given by mass fits. The resulting integrated cross sections are given in Table 2. The errors quoted are statistical only.

The main sources of systematic errors are the uncertainties in the background contribution and acceptance calculation. We use the variation of background yields when passing from formulation (10) to fifth-order polynomials as an estimate of the relative background uncertainty due to its shape. It was found to be in the range from 10 to 20%. The systematic errors for acceptance calculation come from the uncertainties in the track reconstruction and trigger efficiency as well as from the variations of the particle spectra and angular distributions generated by Monte Carlo. The former have been estimated to be less than 20% by comparing the WA56 quasi-two-body reaction cross sections at 12 GeV/c [19] with those of [20], while the latter have been evaluated to be about 20% and 30% for reactions (4), (6) and (5), (7), respectively, by varying the slopes of the u' distributions, and allowing deviations from the decay isotropy (we used $dN/d\cos\theta_J \propto \sin^2\theta_J$ and $dN/d\cos\theta_J \propto \cos^2\theta_J$; θ_J was defined in Sect. 2.4).

The uncertainties due to production mechanisms greatly increase when trying to calculate the experimental acceptance for the six final-state particles of the 5-prong reaction (8), since the large number of parameters to be varied makes the model become ill defined. Therefore, rather than deriving a value we prefer to quote a range of 5–30 nb for the cross section of the 2020 $p\overline{p}$ state produced in this reaction.

As shown in Table 3 and discussed in Sect. 6, our 12 GeV/c cross section for production of the 2020 $p\overline{p}$ state in reaction (6) corresponds to the one found by Benkheiri et al. [1], corrected by the ratio of their acceptance calculated for backward production of this state, and the same, recalculated by us for central production.

Table 3. The cross sections measured in the pioneer experiment of Benkheiri et al. [1] and in the WA56 experiment, both for 4-prong, 4-constraint events [2] and for channels with a missing pion (this work), are mutually compatible (numbers given in bold characters) only if a central production mechanism is assumed, and only for the 2020 peak. The 2200 peak of [1] has not been seen in WA56 (nor in any other experiment)

$[p\overline{p}]$ mass (MeV/c^2)	2020			2200	
Backward production					
Reference	[1]	[2]		[1]	[2]
Reaction $\pi^- p \to \Delta(1232)[p\overline{p}]$					
Acceptance (%)	45	6		23	6
σ (nb)	10±4	<2		21±5	<3
Reaction $\pi^- p \to N(1520)[p\overline{p}]$					
Acceptance (%)	18	4			4
σ (nb)	26±8	<2			<8
Central production, (re)computed by us					
Reaction $\pi^- p \to p_f[p\overline{p}]\pi_s^-$					
Reference	[1]	[2]	This work	[1]	This work
Acceptance (%)	8	1	2.4	8	7.2
σ (nb)	**124±33**	**100±35**	**84±22**	140±33	<30

However, the second $p\overline{p}$ state at a mass of 2.20 GeV/c^2, reported in [1], is nowhere seen in our data. Assuming central production of this state, we have calculated the upper limits for its production cross sections to be 10 nb in reaction (4) (3-prong reactions at 20 GeV/c) and 30 nb in reaction (6) (3-prong reactions at 12 GeV/c), at 95% CL.

5 Baryonium signature of the observed $p\overline{p}$ state

Besides the $p\overline{p}$ decay channel of the 2020 resonance, we have investigated also the mesonic $\pi^+\pi^-$, $2\pi^+2\pi^-$, $\pi^+\pi^-\pi^0$ and K^+K^- final states, produced centrally in the baryon exchange reactions:

$$\pi^\pm p \to p_f \pi^+\pi^-(\pi_s^\pm), \quad (13)$$

$$\pi^\pm p \to p_f 2\pi^+2\pi^-(\pi_s^\pm), \quad (14)$$

$$\pi^\pm p \to p_f \pi^+\pi^-(\pi^0)\pi_s^\pm, \quad (15)$$

$$\pi^\pm p \to p_f K^+K^-(\pi_s^\pm) \quad (16)$$

at 20 (12) GeV/c incident π^+ (π^-) momenta. No peaks at 2.02 GeV/c^2 were found in any of the reactions (13)–(16). In order to illustrate the behavior of the data in the vicinity of the 2.02 GeV/c^2 mass, we show in Fig. 9 the $\pi^+\pi^-$ and $2\pi^+2\pi^-$ mass spectra from reactions (13) and (14). Only ρ^0 and f_2 signals are seen, in the $\pi^+\pi^-$ spectra, a feature described in [7,19] (the difference in ratios between f_2 and ρ^0 production rate can be related to different couplings in the double baryon exchange processes induced by π^+ and π^-). The upper limits for the 2020 state production cross sections multiplied by the mesonic branching ratios are given in Table 2.

At 20 GeV/c, an upper limit for a radiative decay of the 2020 state is also given. Such a decay could compete with the $p\overline{p}\pi^0$ final state, which is almost forbidden by the small amount of phase space available.

Dalkarov et al. [21] proposed a quasi-nuclear approach to explain the results on the reaction $\overline{p}p \to \Lambda\overline{\Lambda}$. In this model, quasi-nuclear states of a mass close to 2 GeV/c^2, if they exist, would decay predominantly into $K^*(892)^0\overline{K^*}(892)^0$, and marginally into $p\overline{p}$ final states [22]. In order to verify this possibility, we have tried to find the 2020 signal in the $K^*\overline{K^*}$ final states in the baryon exchange reaction

$$\pi^+ p \to p_f K^+\pi^-K^-\pi^+(\pi_s^+) \quad (17)$$

with the same method as described above.

No signal was found in the $K^+K^-\pi^+\pi^-$ nor in the $K^*(892)^0\overline{K^*}(892)^0$ mass spectra. This gives an upper limit for the cross section of the production of the 2020 state decaying into $K^*(892)^0\overline{K^*}(892)^0$, quoted in Table 2, which is at the same level as the $p\overline{p}$ value. The value contains a factor 2^2 to take into account the unseen neutral decay modes of the K*s.

On the other hand, plotting the missing-mass spectrum to the $p_f\pi^+$ in the 2-prong topology of the π^+p exposure, i.e. searching for neutral decays of the 2020 peak via reaction (9), we have found a four-standard deviation peak centered at 2.01 GeV/c^2 (shown in Fig. 10), when using selection criteria favoring the neutral system to be in the central region (missing momentum $p_{\rm mis} > 2$ GeV/c, and longitudinal momentum of π^+, $p_l^{\pi^+} < 0.4$ GeV/c). This 2-prong topology channel is singled out by the absence of the

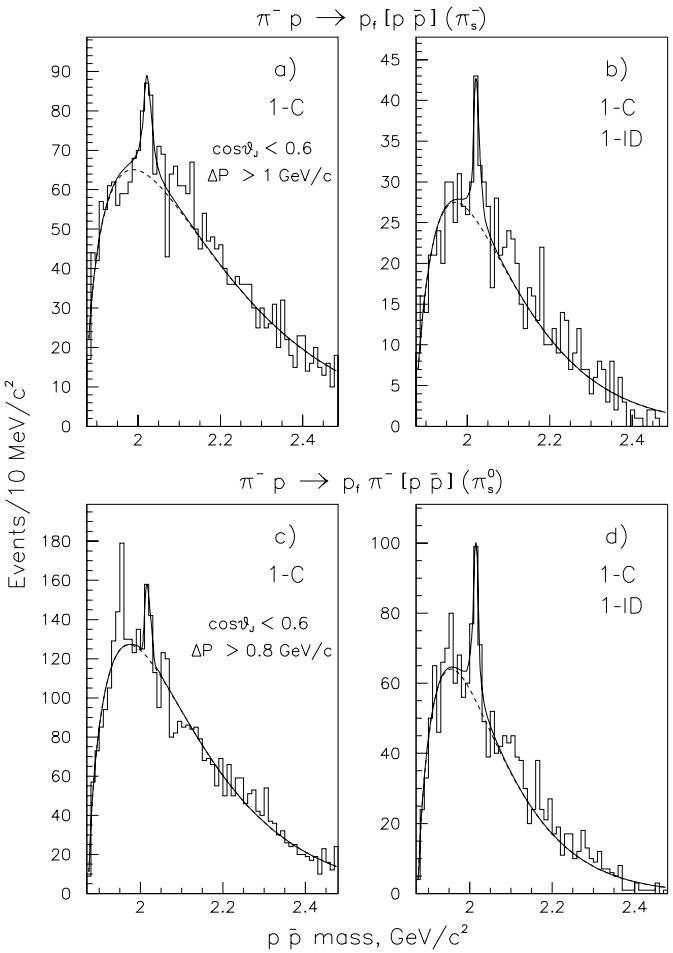

Fig. 6a–d. $p\bar{p}$ mass spectra for 1-C events from **a** reaction (6), events, satisfying kinematic cuts; **b** events from reaction (6) with the $\bar{p}$ identified by the TOF and/or barrel hodoscope; **c**, **d** the same as **a**, **b** but for reaction (7). The "1-ID" indicates that one final state particle (here the $\bar{p}$) is identified

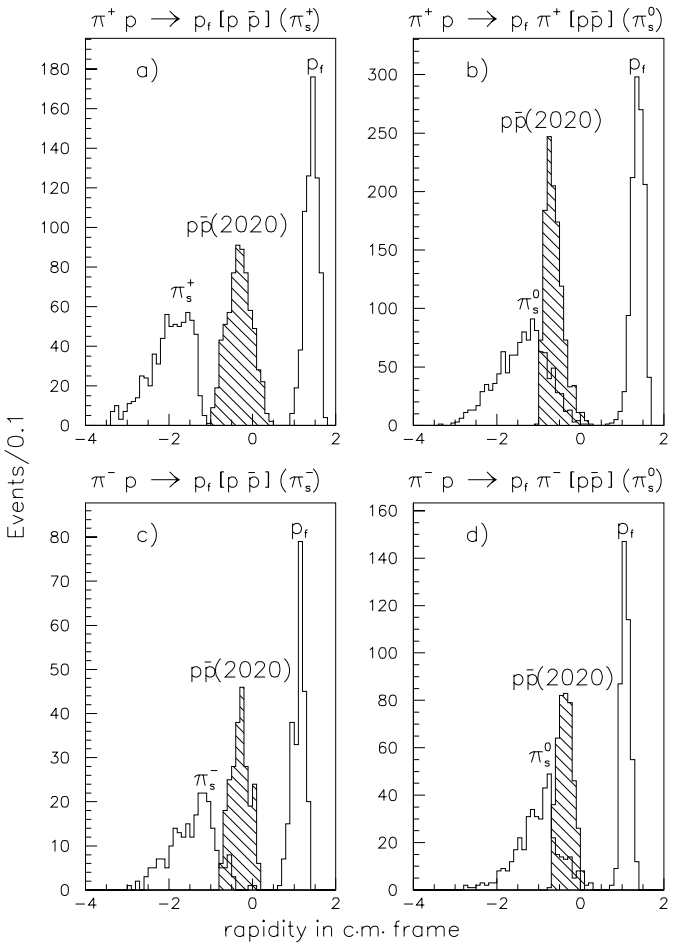

Fig. 8a–d. Rapidity spectra for fast protons, slow pions and $p\bar{p}$ system for 1-C events passed kinematic cuts, $2.00 < M_{\bar{p}p} < 2.03$ GeV/c^2, from reactions (4)–(7), respectively

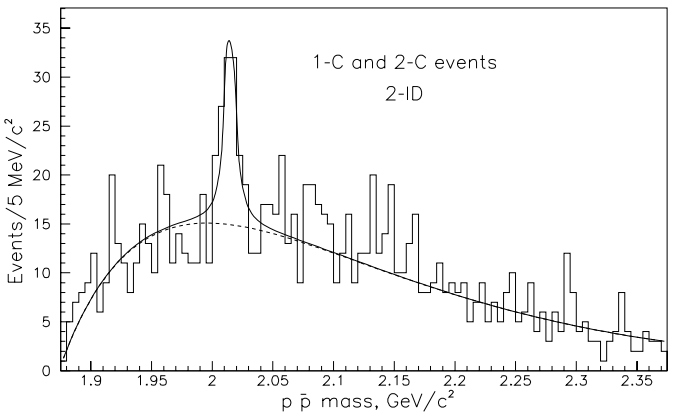

Fig. 7. Combined $p\bar{p}$ mass spectrum for all 2-C, 3-prong and 1-C, 4-prong events (from both π^+p and π^-p runs), in which both p and $\bar{p}$ were identified

diffractive background. The peak width ($\Gamma \simeq 35\,\mathrm{MeV}/c^2$) agrees with the missing-mass resolution in this mass range ($\sigma_{\mathrm{MM}} \simeq 28\,\mathrm{MeV}/c^2$) expected from the Monte Carlo simulation. We interpret this signal as evidence for the decay of the 2020 state into neutrals. The branching ratio for this decay mode was found to be about 2 times higher than the expected branching to the $n\bar{n}$ channel alone (see Table 2); however, the systematic error, mainly due to the uncertainty in the trigger and slow pion track reconstruction efficiencies, reaches 30% and could explain this difference, therefore the evidence for unseen mesonic channels is not compelling. Hence we derive an upper limit for the partial width of all neutral mesonic modes roughly equal to the total width of the two $N\bar{N}$ modes.

From these results and taking into account the small width of the observed 2020 $p\bar{p}$ state, we believe that it is a firm baryonium candidate, i.e. an exotic resonant state, strongly coupled to baryons and decoupled from mesons, of the kind postulated earlier by various authors [13–16].

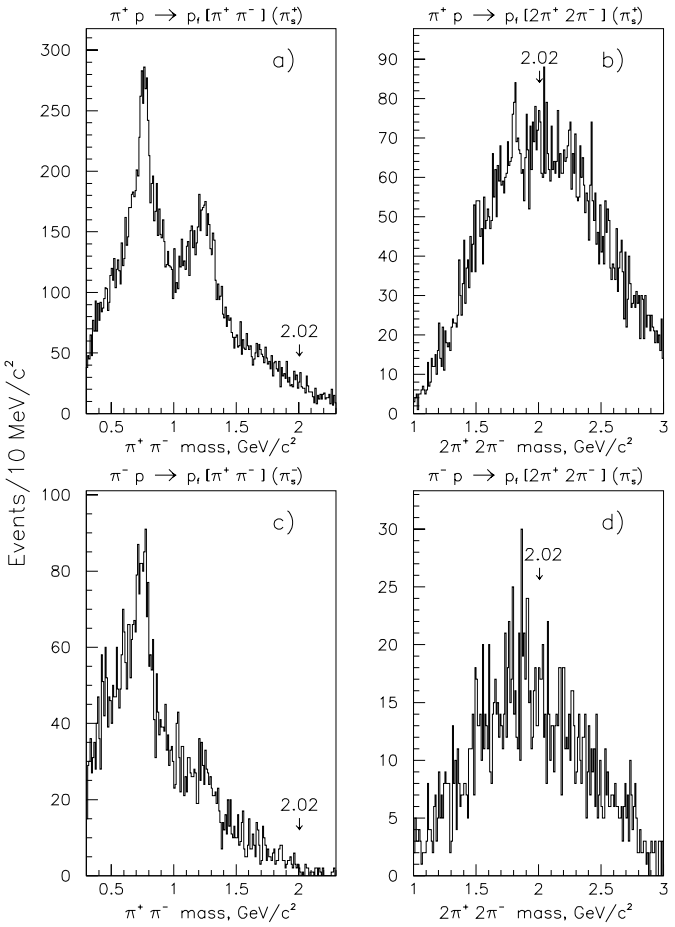

Fig. 9a–d. Pionic mass spectra, for upper limits to pionic decays of the 2020 state, from 1-C events; **a**, **b** for π^+p, **c**, **d** for π^-p reactions; **a** and **c** for $\pi^+\pi^-$, **b** and **d** for $2\pi^+2\pi^-$ decay mode

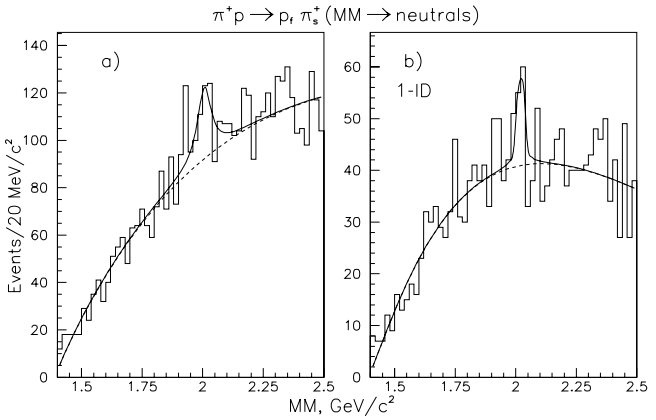

Fig. 10a,b. Missing-mass spectrum for events of ++ topology in the 20 GeV/c π^+p exposure, reaction (9), surviving the following cuts: **a** missing momentum $p_{\rm mis} > 2\,{\rm GeV}/c$, longitudinal momentum of π^+, $P_{l\pi^+} < 0.4\,{\rm GeV}/c$; **b** the same, with the $\pi_{\rm s}^+$ identified by the barrel hodoscope

6 Are all experimental results on the 2.02 GeV/c^2 pp̄ state compatible?

We will discuss in turn the compatibility of the 2020 peak with published production experiments, upper limits from published formation experiments and what they tell us about the 2020 baryonium candidate; and finally, ideas on what future experiments might focus on.

6.1 Production experiments

Apparently, the set of the experimental results on the 2020 p$\overline{\rm p}$ state in production experiments looks controversial, containing claims pro and contra. However, they can be put into accordance by considering that all the results on production cross sections (or on upper limits) depend strongly on the reaction mechanism assumed for calculating the experimental acceptances. This appears to be a point of considerable importance, since widely differing cross sections can be obtained using the same number of fitted events. With this possibility in mind we may proceed to review the experimental results on the production of the 2020 p$\overline{\rm p}$ state.

First of all, the two most obvious problems must be solved: the original WA56 evidence against the 2020 p$\overline{\rm p}$ state [2] confronted with the observation of Benkheiri et al. [1], and the inner compatibility of the WA56 results (earlier negative evidence [2] confronted with the present positive one).

We start with the results on the production cross section of Benkheiri et al. [1] for the 12 GeV/c π^- run. They calculated experimental acceptances assuming backward production of the 2020 p$\overline{\rm p}$ state. To get a proper comparison of the results, we have recalculated the acceptance of their apparatus using our central production mechanism model, as mentioned in Sect. 4, and found it to be essentially smaller, as shown in Table 3. The correspondingly revised cross section of $(124 \pm 33 \pm 20)$ nb is in agreement with ours, which is $(84 \pm 22 \pm 20)$ nb.

The reasons are easy to understand. A p$\overline{\rm p}$ state produced backward in the c.m. frame (see diagram 2a) is going forward in the lab, and imparts to its decay fragments, p and $\overline{\rm p}$, enough longitudinal momentum to ensure their effective detection, together with the fast pion (π^- in diagram 2a). Thus, all outgoing particles in a p$\overline{\rm p}$ backward production process are easily detectable. This is not the case for the central production of this system in reactions (4)–(9) (as an example, see diagram 2c). Here the backward produced particles are low-momentum pions, which go mainly backward in the lab frame too. Such pions may escape detection if the experimental setup is not designed properly to catch them.

Similarly, the 4-prong acceptance of the WA56 apparatus calculated in terms of the central production is a factor of 10 smaller than the one for backward production. Using the p$\overline{\rm p}$ spectrum from the 20 GeV/c π^+p run shown in Fig. 3b of [2] (before selection of the recoil $\rm p_f\pi^+$ system mass in the $\Delta^{++}(1232)$ region) one can obtain an upper limit of 30 nb (at 95% C.L.) for the 2020 p$\overline{\rm p}$ state which should be compared with the $(23 \pm 4 \pm 5)$ nb cross section

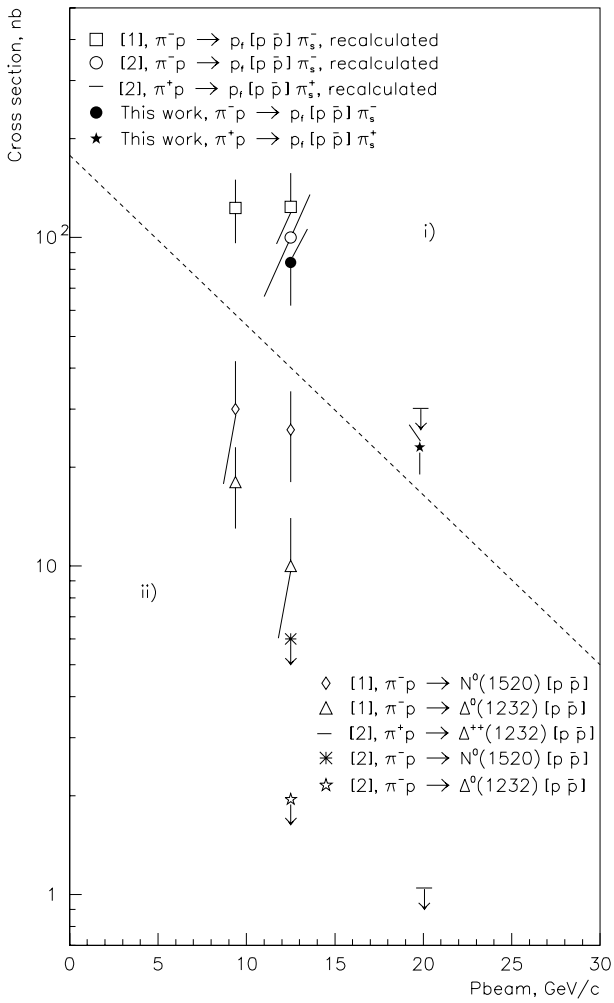

Fig. 11. Cross sections for production of the 2020 $p\bar{p}$ state from the Benkheiri et al. [1] and WA56 experiment ([2] and this work). When analyzed as backward production (below the dashed line), the positive results of [1] were contradicted by the much lower upper limits of [2]. Reanalyzed as central production (above the dashed line), the cross section values are higher, reflecting the lower acceptance, and they are compatible with each other, as well as with the new topologies used in the present work. See also the text and Table 3

reported in this work for reaction (4). As to the 12 GeV/c π^-p exposure, some irregularity around 2.02 GeV/c^2 can be seen in the $p\bar{p}$ mass distribution in Fig. 2b of [2]. The number of events of this effect (60±21) corresponds to a cross section of 100 nb for the 2020 $p\bar{p}$ state, which is again compatible with our value of (84±22 ± 20) nb for reaction (6), as shown in Fig. 11.

Thus, consistency is obtained for the set of basic results on the production of the 2020 $p\bar{p}$ state in the baryon exchange experiments reported here as well as in [1,2]. As to the other baryon exchange experiments [3–6], their lower sensitivities and weaker restrictions imposed on the 2020 $p\bar{p}$ state readily explain the claimed absence of the 2020 $p\bar{p}$ state. Note also the observation of a 2 s.d. signal around 2.02 GeV/c^2 $p\bar{p}$ mass by Chung et al. [5] originally quoted in [23], but suspected to be a possible reflection of the ρ^0 meson contaminating the $p\bar{p}$ spectrum. The same group reported also the negative results of the search for narrow $p\bar{p}$ states in reactions $\bar{p}p \to (p\bar{p})_f\pi^0$ and $\bar{p}p \to (p\bar{p})_f\rho^0$ at 5 GeV/c [24]. These reactions are dominated by baryon exchange, and are in fact crossed backward production processes. We note in passing that in the reaction with a ρ^0 meson, a 2 s.d. signal was seen at a $p\bar{p}$ mass near 2.02 GeV/c^2, with a corresponding production cross section of (150 ± 80) nb.

Also some irregularities at 2.02 GeV/c^2, at small signal-to-background ratios and with statistical significance varying from 2 to 3 s.d., can be seen in the $p\bar{p}$ spectra of experiments which aimed to study the $p\bar{p}$ system produced diffractively in π^-p interactions at 16 GeV/c [25], in π^+p interactions at 50 GeV/c [26] and in pp interactions at 11.75 GeV/c [27], and of the experiment of [28] with $\bar{p}p$ interactions at 12 GeV/c. Unfortunately, these results cannot be quantitatively compared with those of baryon exchange experiments because of the lack of the data necessary to calculate acceptances based on a given production mechanism.

Such a comparison can be done for the Omega experiment of Beusch et al. [29] who explored the central region in π^-p and π^+p induced reactions at 40 GeV/c. The upper limits for the central production of the 2020 $p\bar{p}$ state are quoted to be about 36 nb in this experiment. For example, a small bump at 2.02 GeV/c^2 seen in the π^-p data corresponds to a production cross section of (22 ± 12) nb.

We note also indications on the $p\bar{p}$ structure in the mass region close to 2.02 GeV/c^2 in experiments on $p\bar{p}$ electroproduction at 11.5 GeV [30], and on $p\bar{p}$ photoproduction at 4.7–6.6 GeV [31].

We summarize all these results, including our own, in Table 4. Those hadron beam experiments which give positive indications for the 2020 $p\bar{p}$ state, and for which production cross sections are known or could be calculated, are shown in Fig. 12, together with the upper limit for its central production in 20 GeV/c, the 4-C channel data of [2].

We finish the review of the production experiments on the 2020 state by recalling that a charged narrow state of this mass decaying into $p\bar{n}$ and $\bar{p}n$ has also been reported [32]. These authors claim that the state is not peripherally produced, which effectively implies that the central production mechanism is favored. Unfortunately, with our data we have no possibility to look for this charged state since its central production (and subsequent decay to the $p\bar{n}$ and $\bar{p}n$) would assume two particles going undetected in our experimental configuration (neutron and slow pion). As to the backward production of this charged state, upper limits are given in [33].

6.2 Formation experiments, and the width of the 2.02 GeV/c^2 $p\bar{p}$ state

The 2.02 GeV/c^2 mass region has been investigated in $p\bar{p}$ formation experiments near the corresponding $p_{\bar{p}} \simeq$ 800 MeV/c (albeit not as extensively as an early $p\bar{p}$ can-

Table 4. The $p\overline{p}(2020)$ signals (mass, width and number of standard deviations) seen in relevant channels of the Benkheiri et al. [1] and WA56 experiment, as well as other production experiments. All results in the table are statistically independent

or Figure	Reaction		$P_{\rm beam}$ (GeV/c)	Mass (MeV/c^2)	Width (MeV/c^2)	n.s.d.
A. Results from Benkheiri et al. [1] and WA56 experiment ([2] and this work)						
Benkheiri et al. [1]	$\pi^-p \to p_f[p\overline{p}]\pi_s^-$	4-C	9	2020±3	24± 12	4.7
			12			3.8
Ajaltouni et al. [2]	$\pi^-p \to p_f[p\overline{p}]\pi_s^-$	4-C	12	2020	≤20	2.9
6a; also [8]	$\pi^-p \to p_f[p\overline{p}](\pi_s^-)$	1-C	12	2024±5	22±15	3.8
6c; also [8]	$\pi^-p \to p_f\pi^-[p\overline{p}](\pi_s^0)$	1-C	12	2015±4	15±9	4.4
4a; also [8]	$\pi^+p \to p_f[p\overline{p}](\pi_s^+)$	1-C	20	2009±6	30±12	6.0
4c; also [8]	$\pi^+p \to p_f\pi^+[p\overline{p}](\pi_s^0)$	1-C	20	2012±6	34±21	7.0
5f	$\pi^+p \to p_f2\pi^+[p\overline{p}](\pi_s^-)$	1-C	20	2010±8	11±7	3.5
10a	$\pi^+p \to p_f\pi_s^+$[neutrals]		20	2007±9	∼30	4.0
B. Results from other experiments						
Chung et al. [23]	$\pi^-p \to p_f\pi^-[p\overline{p}]$	4-C	16	2020	≤20	2.0
Chung et al. [24]	$\overline{p}p \to [p\overline{p}]_f\rho^0$		5	2010	≤10	1.8
Armstrong et al. [25]	$\pi^-p \to [p_f\overline{p}]\pi^-p_s$	4-C	16	2025	≤10	2.4
Cleland et al. [26]	$\pi^-p \to [p_f\overline{p}]\pi^-p_s$	4-C	50	2025	≤10	3.1
Kooijman et al. [27]	$pp \to p[p\overline{p}]p_s$	3-C	11.75	2025	≤10	1.8
Armstrong et al. [28]	$\overline{p}p \to [p_f\overline{p}_f]\pi^+\pi^-$	1-C	12	2030	≤15	2.3
Beusch et al. [29]	$\pi^-p \to [p\overline{p}]_{\rm cent} + X^0$		40	2020	≤5	1.8
Gibbard et al. [30]	$e^-p \to e^-[p\overline{p}]p$	4-C	11.5	2020	≤40	2.3
Bodenkamp et al. [31]	$\gamma p \to [p\overline{p}]p_s$	1-C	4.7-6.6	2023±5	27±12	1.7

didate, once called S-meson, near 1.94 GeV/c^2). Four experiments scanned this region in fine steps: [34,35] studied the total and charged annihilation cross sections, [36] the backward elastic cross section, and [37] charge exchange ($p\overline{p} \to n\overline{n}$). No signal of the 2020 state was found; the most accurate restrictions result from the charge-exchange experiment [37] (see below). From their results, an important conclusion about the width of the 2020 state can be drawn using the relation between observable production cross section $\sigma_{\rm exp}^{p\bar{p}\to n\bar{n}}$ of a resonance having a mass 2.02 GeV/c^2, and its other quantum numbers such as spin J, elasticity $\beta_{N\bar{N}}$ and width Γ:

$$\sigma_{\rm exp}^{p\bar{p}\to n\bar{n}}(2.02) \simeq (2J+1)\beta_{N\bar{N}}^2 \times 2.25\,{\rm mb} \times \frac{\Gamma}{2\Delta}\arctan\frac{2\Delta}{\Gamma}, \qquad (18)$$

where Δ is the experimental mass resolution (see the Appendix).

From [37] an upper limit of 0.2 mb can be derived for $\sigma_{\rm exp}^{p\bar{p}\to n\bar{n}}(2.02)$[2]. The experimental resolution Δ of [37] was $\simeq 2\,{\rm MeV}/c^2$. Confronting these values with the estimation (A.4) of the Appendix and with formula (18), one can conclude that the width of the 2020 state is essentially smaller than the quoted resolution (unless the elasticity $\beta_{N\bar{N}}$ is much smaller than 1, which seems to be excluded by the fact that it is hardly seen in mesonic final states, see Sect. 5). Thus, from (18) we get the inequality

$$(2J+1)\beta_{N\bar{N}}^2\Gamma \le 0.23\,{\rm MeV/c^2}. \qquad (19)$$

Assuming $\beta_{N\bar{N}} = 1$ one gets for $J = 0$

$$\Gamma_0 \le 230\ {\rm keV/c^2}, \qquad (20)$$

and for $J = 2$

$$\Gamma_2 \le 50\ {\rm keV/c^2}. \qquad (21)$$

One may relax somewhat these restrictions, supposing that a real baryonium can decay into mesonic channels as well ($\beta_{N\bar{N}} < 1$). However, even with $\beta_{N\bar{N}} = 0.5$, the Γ upper limits (20) and (21) become 1 MeV/c^2 and 200 keV/c^2 respectively, which are still essentially smaller than the best experimental limit of $\Gamma \le 10\,{\rm MeV}/c^2$ resulting from the fit of our combined spectrum, Sect. 3.3. This was already noted in [38].

Apparently, such a small width is not compatible with predictions of the quasi-nuclear models [21,39]. However, it can be adjusted to the quark models of baryonia [10–16], which still have much space to develop.

[2] A similar limit ($\simeq$ 0.3 mb) can be derived from the differential elastic cross section $d\sigma/d\Omega$ of [36], measured at $\cos(\theta_{c.m.}) = -0.994$, with $\Delta = 3\,{\rm MeV}/c^2$, if one assumes isotropic decay of the $p\overline{p}$ resonant state

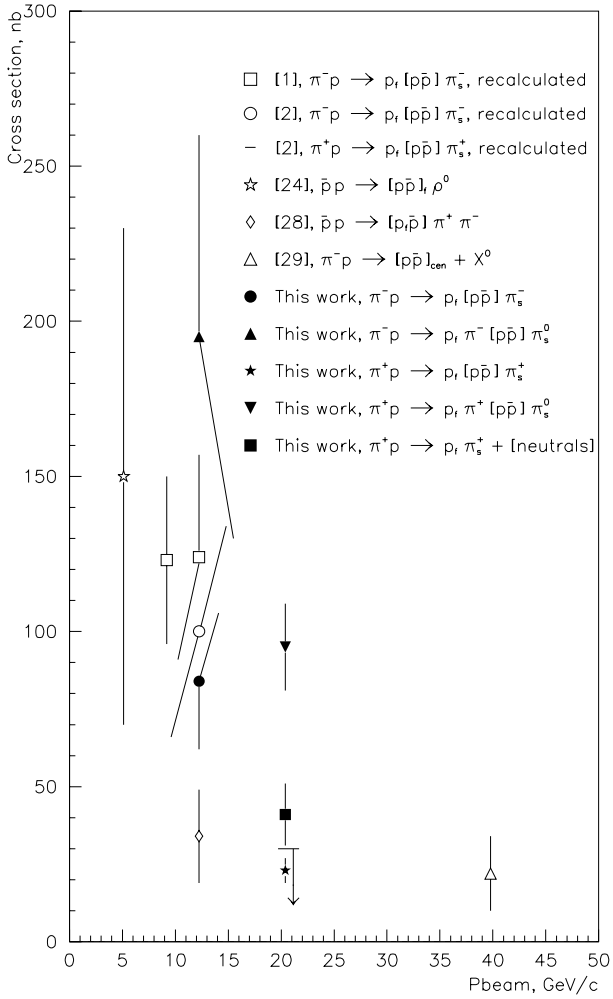

Fig. 12. Summary of hadronic production cross sections for the 2020 $p\overline{p}$ state, from [1,2,24,28,29], and from the present work. The cross sections of Benkheiri et al. [1] and Ajaltouni et al. [2] have been corrected on the basis of our central production model. The errors shown are statistical, and do not include systematic uncertainties, which vary from 15% to 30%. See also Table 4

6.3 Remark on the production mechanism of the 2.02 GeV/c^2 $p\overline{p}$ state

While the double baryon exchange mechanism of (central) production of the 2020 state is capable to put into accordance the set of the experimental results discussed above, the reason why this mechanism dominates over the backward production, i.e. the production through single baryon exchange, has to be explained. Indeed, the central production of ordinary mesons also shows a prevalence over their backward production [7], but the enhancement factor does not exceed 4 in that case, whereas for the 2020 $p\overline{p}$ state production this factor is at least 20, as one can see comparing the central production cross sections reported here and the upper limits for the backward production cross sections given in [2].

A simple way to explain such a peculiarity of the measured cross sections, together with the narrowness of the observed $p\overline{p}$ state is to assume that this state is coupled to $\Delta\overline{\Delta}$ much stronger than to $N\overline{N}$. If this assumption is true, processes of backward production of the 2020 $p\overline{p}$ state, where double delta exchange is excluded, are naturally suppressed, and the dominant processes are of the type plotted in Fig. 2c. The very small width of the observed $p\overline{p}$ state could also be explained with this hypothesis: once being produced in the collision of virtual Δ and $\overline{\Delta}$ this state is not allowed to decay into the real $\Delta\overline{\Delta}$ since its mass is below the corresponding threshold, and it is forced to decay via the suppressed $p\overline{p}$ channel.

The question of double delta exchange dominance in the production of the 2020 $p\overline{p}$ state remains to be settled by future experiments. A careful experimental study of π^-p and $\overline{p}$p baryon exchange reactions, using fast-proton and fast π^+ triggers, respectively, and capable of detecting slow backward produced π^-s is strongly advocated.

7 Conclusion

We have found a narrow $p\overline{p}$ peak at mass $M = 2.015 \pm 0.003\,\mathrm{GeV}/c^2$, in six different πp baryon exchange reactions with one missing or incompletely reconstructed slow pion. These were $\pi^+p \to p_f[p\overline{p}]\pi_s^+$, $\pi^+p \to p_f\pi^+[p\overline{p}]\pi_s^0$, $\pi^+p \to p_f\pi^+\pi^+[p\overline{p}]\pi_s^-$ and $\pi^+p \to p_f\pi_s^+[\mathrm{MM} \to \mathrm{neutrals}]$ at 20 GeV/c; and $\pi^-p \to p_f[p\overline{p}]\pi_s^-$ as well as $\pi^-p \to p_f\pi^-[p\overline{p}]\pi_s^0$ at 12 GeV/c. For this we had reanalyzed the available WA56 data. The evidence for the neutral decay mode of the observed state led to a branching ratio close to the $p\overline{p}$ one. Since no explicit mesonic decay modes of this state were seen, we conclude that the observed state is a baryonium candidate, decaying only reluctantly to mesons.

Its mass and width are in a good agreement with those of a state found by Benkheiri et al. [1] in an earlier baryon exchange experiment, also done at the Omega spectrometer. The large difference between the production cross sections obtained here and those of [1] is reduced when we recompute the cross section of [1] assuming that the state is produced centrally, as seen in our data, rather than backwards in the c.m. The same dominantly central production can explain why backward production experiments [2–6] have failed to confirm this state, including Ajaltouni et al. [2], who had analyzed the 4-constraint events of the WA56 experiment. The non-observation of the state in formation experiments done so far is quantitatively understandable if its real width is near 1 MeV/c^2 or less.

We hope that this work may find its use as a basis to renewed baryonium spectroscopy in future hadronic experiments with high resolution and sensitivity. A baryon exchange trigger is a must in production experiments, while in formation experiments the step width ($\sim 100\,\mathrm{keV}/c^2$) is the crucial feature.

Acknowledgements. We are grateful to A. Kaidalov, V. Markushin and L. Montanet for useful discussions. V.F.P. thanks the colleagues from IFIC for their warm hospitality and

help when preparing this paper. The work done by A.A.G. was supported in part by the INTAS grant No. 93-0079 and by the Generalitat Valenciana visitor's Grant.

Appendix

The contribution of a resonance with a spin J to the cross section of the process $1+2 \to 1'+2'$ (formation process) has the form [40]

$$\sigma_{\mathrm{BW}}(E) = \frac{2J+1}{(2S_1+1)(2S_2+1)}, \times \frac{\pi}{k^2} \frac{B_{\mathrm{in}} B_{\mathrm{out}} \Gamma_{\mathrm{tot}}^2}{(E-E_{\mathrm{R}})^2 + \Gamma_{\mathrm{tot}}^2/4}. \quad (A.1)$$

For $N\bar{N} \to N\bar{N}$ at $E = E_{\mathrm{R}}$ one has

$$\sigma_{\mathrm{BW}}^{N\bar{N}\to N\bar{N}}(E_{\mathrm{R}}) = (2J+1) B_{N\bar{N}}^2 \frac{\pi}{k_{\mathrm{R}}^2}. \quad (A.2)$$

At $E_{\mathrm{R}} = 2.02$ one has $k_{\mathrm{R}} \simeq 0.37\,\mathrm{GeV}/c$ and thus

$$\sigma_{\mathrm{R}}^{N\bar{N}\to N\bar{N}}(E_{\mathrm{R}} = 2.02) \simeq (2J+1) B_{N\bar{N}}^2 \times 23\,\mathrm{GeV}^{-2} \simeq (2J+1) B_{N\bar{N}}^2 \times 9.0\,\mathrm{mb}. \quad (A.3)$$

Now, for the $p\bar{p} \to p\bar{p}$ process, taking into account the nucleon isospin Clebsch–Gordan factor, we have an estimate for the cross section at maximum (the same would be true for the $p\bar{p} \to n\bar{n}$ reaction):

$$\sigma_{\mathrm{R}}^{p\bar{p}\to p\bar{p}}(E_{\mathrm{R}} = 2.02) \simeq (2J+1) \beta_{N\bar{N}}^2 \times 2.25\,\mathrm{mb}, \quad (A.4)$$

where $\beta_{N\bar{N}}$ is the elasticity ($\beta_{N\bar{N}} = 1$ for an "ideal" baryonium that decays into $p\bar{p}$ and $n\bar{n}$ only).

Let us take into account an experimental resolution $\pm\Delta$. The cross section averaged over the interval 2Δ around E_{R} is (for a narrow resonance)

$$\sigma_{\mathrm{exp}}(E_{\mathrm{R}}) = \frac{1}{2\Delta} \int_{E_{\mathrm{R}}-\Delta}^{E_{\mathrm{R}}+\Delta} \sigma_{\mathrm{BW}}(E)\mathrm{d}E \simeq \sigma_{\mathrm{R}} \times \frac{\Gamma}{2\Delta} \arctan \frac{2\Delta}{\Gamma}. \quad (A.5)$$

Thus,

$$\sigma_{\mathrm{exp}}^{p\bar{p}\to p\bar{p}}(2.02) \simeq (2J+1) \beta_{N\bar{N}}^2 \times 2.25\,\mathrm{mb} \times \frac{\Gamma}{2\Delta} \arctan \frac{2\Delta}{\Gamma}. \quad (A.6)$$

References

1. P. Benkheiri et al., Phys. Lett. B **68**, 483 (1977)
2. Z. Ajaltouni et al., Nucl. Phys. B **209**, 301 (1982)
3. R.M. Bionta et al., Phys. Rev. Lett. **44**, 909 (1980)
4. A.S. Carroll et al., Phys. Rev. Lett. **44**, 1572 (1980)
5. S.U. Chung et al., Phys. Rev. Lett. **45**, 1611 (1980)
6. A.D.J. Banks et al., Phys. Lett. B **100**, 191 (1981)
7. V.F. Perepelitsa et al., Z. Phys. C **52**, 407 (1991)
8. A. Ferrer et al., Proceedings of the 2nd Biennial Conference on Low Energy Antiproton Physics LEAP'92, Courmayer, 1992; Nucl. Phys. A **558**, 191c (1993)
9. A. Ferrer et al., Proceedings of the 6th International Conference on Hadron Spectroscopy HADRON'95, Manchester, 1995, edited by M.C. Birse, G.D. Lafferty, J.A. McGovern (World Scientific, Singapore, 1996), p. 460
10. G.C. Rossi, G. Veneziano, Nucl. Phys. B **123**, 507 (1977)
11. M. Imachi, S. Otsuki, F. Toyoda, Progr. Theor. Phys. **57**, 517 (1977)
12. Chan Hong-Mo et al., Phys. Lett. B **76**, 634 (1978)
13. Chan Hong-Mo, H. Högaasen, Phys. Lett. B **72**, 121, 400 (1977); Nucl. Phys. B **136** 401 (1978)
14. M. Uehara, Progr. Theor. Phys. **61**, 1137 (1979)
15. G.C. Rossi, G. Veneziano, Phys. Rep. **63**, 153 (1980)
16. Chan Hong-Mo, Nucl. Phys. A **335**, 219 (1980)
17. R. Ehrlich, R.J. Plano, J.B. Whittaker, Phys. Rev. Lett. **20**, 686 (1968)
18. A. Ferrer et al., Phys. Lett. B **394**, 395 (1997)
19. A. Ferrer et al. (to be published)
20. A. Ferrer et al., Nucl. Phys. B **142**, 77 (1978)
21. O.D. Dalkarov, K.V. Protasov, Sov. JETP Lett. **46**, 329 (1987) O.D. Dalkarov, K.V. Protasov, I.S. Shapiro, Int. J. Mod.Phys. A **5**, 2155 (1990)
22. O.D. Dalkarov (private communication)
23. S.U. Chung et al., Proceedings of the 6th International Conference on Experimental Meson Spectroscopy-1980, Brookhaven, 1980, edited by S.U. Chung, S.J. Lindenbaum (AIP, New York, 1981), p.170
24. S.U. Chung et al., Phys. Rev. Lett. **46**, 395 (1981)
25. T.A. Armstrong et al., Phys. Lett. B **85**,304 (1979)
26. W.E. Cleland et al., Phys. Lett. B **86**, 409 (1979)
27. S. Kooijman et al., Phys. Rev. Lett. **45** 316 (1980)
28. T.A. Armstrong et al., Status Report on WA49, CERN/SPSC/79-82 SPSC/M.190, 1979 (unpublished)
29. W. Beusch et al., Talk on the XXI International Conference on High Energy Physics, Paris, 1982 (unpublished)
30. B.G. Gibbard et al., Phys. Rev. Lett. **42**, 1593 (1979)
31. J. Bodenkamp et al., Phys. Lett. B **133**, 275 (1983)
32. F. Azooz et al., Phys. Lett. B **122**, 471 (1983)
33. P. Benkheiri et al., Phys. Lett. B **81**, 380 (1979)
34. R.P. Hamilton et al., Phys. Rev. Let. **44**, 1182 (1980)
35. T. Sumioshi et al., Phys. Rev. Lett. **49**, 628 (1982)
36. M. Alston-Garnjost et al., Phys. Rev. Lett. **43**, 1901 (1979)
37. R.P. Hamilton et al., Phys. Rev. Let. **44**, 1179 (1980)
38. V. Perepelitsa, Proceedings of the 6th International Conference on Hadron Spectroscopy HADRON'95, Manchester, 1995, edited by M.C. Birse, G.D. Lafferty, J.A. McGovern (World Scientific, Singapore, 1996), p.380
39. L.N. Bogdanova, O.D. Dalkarov, I.S. Shapiro, Ann. Phys. **84**, 261 (1974); Sov. JETP **43**, 417 (1976)
40. Review of Particle Properties, Phys. Rev. D **54**, 178 (1996)